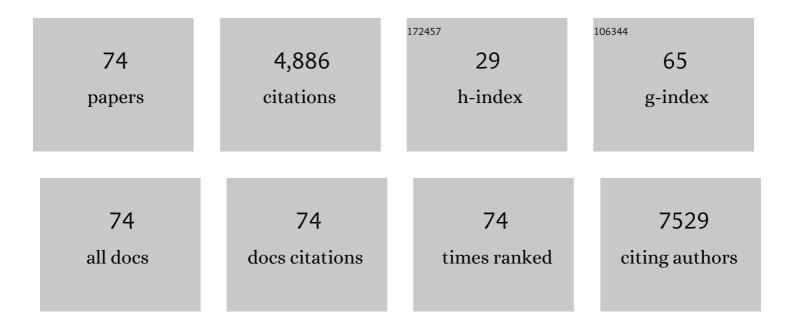
Yunguo Li

List of Publications by Year in descending order

Source: https://exaly.com/author-pdf/5373474/publications.pdf Version: 2024-02-01



ΥμησιοΙ

#	Article	IF	CITATIONS
1	ElasT: A toolkit for thermoelastic calculations. Computer Physics Communications, 2022, 273, 108280.	7.5	3
2	Pressure-tuned one- to quasi-two-dimensional structural phase transition and superconductivity in <mml:math xmlns:mml="http://www.w3.org/1998/Math/MathML"><mml:msub><mml:mi mathvariant="normal">LiP<mml:mn>15</mml:mn></mml:mi </mml:msub></mml:math> . Physical Review B, 2022, 105, .	3.2	4
3	Nitrogen Speciation in Silicate Melts at Mantle Conditions From Ab Initio Simulations. Geophysical Research Letters, 2022, 49, .	4.0	0
4	Light-emitting field-effect transistors with EQE over 20% enabled by a dielectric-quantum dots-dielectric sandwich structure. Science Bulletin, 2022, 67, 529-536.	9.0	23
5	General Bottom-Up Colloidal Synthesis of Nano-Monolayer Transition-Metal Dichalcogenides with High 1T′-Phase Purity. Journal of the American Chemical Society, 2022, 144, 4863-4873.	13.7	58
6	Regulation of energetic hot carriers on Pt/TiO2 with thermal energy for photothermal catalysis. Applied Catalysis B: Environmental, 2022, 309, 121263.	20.2	38
7	Quasiâ€Shellâ€Growth Strategy Achieves Stable and Efficient Green InP Quantum Dot Lightâ€Emitting Diodes. Advanced Science, 2022, 9, .	11.2	33
8	The effect of water on the outer core transport properties. Physics of the Earth and Planetary Interiors, 2022, 329-330, 106907.	1.9	3
9	Primitive noble gases sampled from ocean island basalts cannot be from the Earth's core. Nature Communications, 2022, 13, .	12.8	6
10	Equation of state for CO and CO2 fluids and their application on decarbonation reactions at high pressure and temperature. Chemical Geology, 2021, 559, 119918.	3.3	0
11	Smoothing the energy transfer pathway in quasi-2D perovskite films using methanesulfonate leads to highly efficient light-emitting devices. Nature Communications, 2021, 12, 1246.	12.8	274
12	Strong shear softening induced by superionic hydrogen in Earth's inner core. Earth and Planetary Science Letters, 2021, 568, 117014.	4.4	29
13	Zero-emission multivalorization of light alcohols with self-separable pure H2 fuel. Applied Catalysis B: Environmental, 2021, 292, 120212.	20.2	5
14	Tuning of electronic and optical properties of a predicted silicon allotrope: Hexagonal silicon <mml:math xmlns:mml="http://www.w3.org/1998/Math/MathML"><mml:mrow><mml:mi>h</mml:mi><mml:mn>10-Si. Physical Review B, 2021, 104, .</mml:mn></mml:mrow></mml:math 	nn><7mml	:mrow>
15	Ni2+/Co2+ doped Au-Fe7S8 nanoplatelets with exceptionally high oxygen evolution reaction activity. Nano Energy, 2021, 89, 106463.	16.0	45
16	Aligning potential differences within carbon nitride based photocatalysis for efficient solar energy harvesting. Nano Energy, 2021, 89, 106357.	16.0	41
17	Superionic iron-hydrogen alloys in Earth's inner core. , 2021, , .		0
18	Pressure-Induced Structural Phase Transition and Superconductivity in NaSn5. Inorganic Chemistry, 2020, 59, 484-490.	4.0	4

Yunguo L

#	Article	IF	CITATIONS
19	Nonepitaxial Goldâ€Tipped ZnSe Hybrid Nanorods for Efficient Photocatalytic Hydrogen Production. Small, 2020, 16, e1902231.	10.0	37
20	A Hydrogen-Initiated Chemical Epitaxial Growth Strategy for In-Plane Heterostructured Photocatalyst. ACS Nano, 2020, 14, 17505-17514.	14.6	41
21	Equation of State of hcp Feâ€Câ€Si Alloys and the Effect of C Incorporation Mechanism on the Density of hcp Fe Alloys at 300ÂK. Journal of Geophysical Research: Solid Earth, 2020, 125, e2020JB020159.	3.4	10
22	The Earth's core as a reservoir of water. Nature Geoscience, 2020, 13, 453-458.	12.9	56
23	Lattice Distortion in Mixed-Anion Lead Halide Perovskite Nanorods Leads to their High Fluorescence Anisotropy. , 2020, 2, 814-820.		33
24	Dominant Polar Surfaces of Colloidal II–VI Wurtzite Semiconductor Nanocrystals Enabled by Cation Exchange. Journal of Physical Chemistry Letters, 2020, 11, 4990-4997.	4.6	8
25	Photocatalytic Hydrogen Production: Nonepitaxial Goldâ€Tipped ZnSe Hybrid Nanorods for Efficient Photocatalytic Hydrogen Production (Small 12/2020). Small, 2020, 16, 2070066.	10.0	0
26	Water Partitioning between Liquid Iron and Silicate Melt. , 2020, , .		0
27	Colloidal Single‣ayer Photocatalysts for Methanolâ€Storable Solar H ₂ Fuel. Advanced Materials, 2019, 31, e1905540.	21.0	39
28	Ab Initio Molecular Dynamics Investigation of Molten Fe–Si–O in Earth's Core. Geophysical Research Letters, 2019, 46, 6397-6405.	4.0	27
29	Superconductivity in the van der Waals layered compound PS2. Physical Review B, 2019, 99, .	3.2	11
30	Spontaneous Formation of Heterodimer Au–Fe ₇ S ₈ Nanoplatelets by a Seeded Growth Approach. Journal of Physical Chemistry C, 2019, 123, 10604-10613.	3.1	7
31	Photocatalysts: Colloidal Singleâ€Layer Photocatalysts for Methanolâ€Storable Solar H ₂ Fuel (Adv. Mater. 49/2019). Advanced Materials, 2019, 31, 1970348.	21.0	0
32	Carbon Partitioning Between the Earth's Inner and Outer Core. Journal of Geophysical Research: Solid Earth, 2019, 124, 12812-12824.	3.4	23
33	Heterostructured WO ₃ @CoWO ₄ bilayer nanosheets for enhanced visible-light photo, electro and photoelectro-chemical oxidation of water. Journal of Materials Chemistry A, 2018, 6, 6265-6272.	10.3	79
34	Mg partitioning between solid and liquid iron under the Earth's core conditions. Physics of the Earth and Planetary Interiors, 2018, 274, 218-221.	1.9	8
35	Exploring configurational degrees of freedom in disordered solids. AIP Conference Proceedings, 2018,	0.4	0
36	Melting properties from <i>ab initio</i> free energy calculations: Iron at the Earth's inner-core boundary. Physical Review B, 2018, 98, .	3.2	43

Yunguo L

#	Article	IF	CITATIONS
37	Photocatalysis: Spontaneous Formation of Noble- and Heavy-Metal-Free Alloyed Semiconductor Quantum Rods for Efficient Photocatalysis (Adv. Mater. 39/2018). Advanced Materials, 2018, 30, 1870296.	21.0	0
38	Pressure-induced structural phase transition in Li4Ge. CrystEngComm, 2018, 20, 5949-5954.	2.6	2
39	A comparative study of metal (Ni, Co, or Mn)-borate catalysts and their photodeposition on rGO/ZnO nanoarrays for photoelectrochemical water splitting. Journal of Materials Chemistry A, 2018, 6, 24149-24156.	10.3	38
40	Spontaneous Formation of Noble―and Heavyâ€Metalâ€Free Alloyed Semiconductor Quantum Rods for Efficient Photocatalysis. Advanced Materials, 2018, 30, e1803351.	21.0	47
41	The elastic properties of hcp-Fe alloys under the conditions of the Earth's inner core. Earth and Planetary Science Letters, 2018, 493, 118-127.	4.4	59
42	Structural diversity and electronic properties in potassium silicides. Journal of Chemical Physics, 2018, 148, 204706.	3.0	11
43	Strain engineering and photocatalytic application of single-layer ReS2. International Journal of Hydrogen Energy, 2017, 42, 161-167.	7.1	30
44	Physical and chemical properties of Cu(<scp>i</scp>) compounds with O and/or H. Dalton Transactions, 2017, 46, 529-538.	3.3	9
45	Review of two-dimensional materials for photocatalytic water splitting from a theoretical perspective. Catalysis Science and Technology, 2017, 7, 545-559.	4.1	345
46	Impurity effects on the grain boundary cohesion in copper. Physical Review Materials, 2017, 1, .	2.4	13
47	A new 2D monolayer BiXene, M ₂ C (M = Mo, Tc, Os). Nanoscale, 2016, 8, 15753-15762.	5.6	46
48	Thermoelasticity of Fe ₇ C ₃ under inner core conditions. Journal of Geophysical Research: Solid Earth, 2016, 121, 5828-5837.	3.4	28
49	Homogeneously dispersed multimetal oxygen-evolving catalysts. Science, 2016, 352, 333-337.	12.6	1,948
50	Interactions of point defects with stacking faults in oxygen-free phosphorus-containing copper. Journal of Nuclear Materials, 2015, 462, 160-164.	2.7	9
51	Gluing together metallic and covalent layers to form Ru ₂ C under ambient conditions. Physical Chemistry Chemical Physics, 2015, 17, 9730-9736.	2.8	9
52	Bond Network Topology and Antiferroelectric Order in Cuprice CuOH. Inorganic Chemistry, 2015, 54, 8969-8977.	4.0	21
53	Communication: Origin of the difference between carbon nanotube armchair and zigzag ends. Journal of Chemical Physics, 2014, 140, 091102.	3.0	13
54	Electronic structures and optical properties of cuprous oxide and hydroxide. Materials Research Society Symposia Proceedings, 2014, 1675, 185-190.	0.1	1

Yunguo L

#	Article	IF	CITATIONS
55	Dynamic stability of the single-layer transition metal dichalcogenides. Computational Materials Science, 2014, 92, 206-212.	3.0	19
56	Tweaking the magnetism of MoS2 nanoribbon with hydrogen and carbon passivation. Nanotechnology, 2014, 25, 165703.	2.6	20
57	The nature of hydrogen in \hat{I}^3 -alumina. Journal of Applied Physics, 2014, 115, .	2.5	15
58	Hydrogen storage in polylithiated BC3 monolayer sheet. Solid State Communications, 2013, 170, 39-43.	1.9	29
59	Metal-decorated graphene oxide for ammonia adsorption. Europhysics Letters, 2013, 103, 28007.	2.0	17
60	Electronic structure, mechanical and optical properties of In2O3 with hybrid density functional (HSE06). Solid State Communications, 2013, 172, 37-40.	1.9	9
61	Electronic, mechanical and optical properties of Y2O3 with hybrid density functional (HSE06). Computational Materials Science, 2013, 71, 19-24.	3.0	32
62	Single-layer MoS2 as an efficient photocatalyst. Catalysis Science and Technology, 2013, 3, 2214.	4.1	271
63	Strain-induced stabilization of Al functionalization in graphene oxide nanosheet for enhanced NH3 storage. Applied Physics Letters, 2013, 102, .	3.3	7
64	Influence of forming process on three-dimensional morphology of TiB2 particles in Al-Ti-B alloys. Transactions of Nonferrous Metals Society of China, 2012, 22, 564-570.	4.2	22
65	Evolution of nickel-rich phases in Al–Si–Cu–Ni–Mg piston alloys with different Cu additions. Materials & Design, 2012, 33, 220-225.	5.1	138
66	The improvement of microstructures and mechanical properties of near eutectic Al–Si multicomponent alloy by an Al–8Zr–2P master alloy. Materials Science & Engineering A: Structural Materials: Properties, Microstructure and Processing, 2012, 531, 55-60.	5.6	21
67	Distribution of TiB2 particles and its effect on the mechanical properties of A390 alloy. Materials Science & Engineering A: Structural Materials: Properties, Microstructure and Processing, 2012, 546, 146-152.	5.6	61
68	Influence of Si and Ti contents on the microstructure, microhardness and performance of TiAlSi intermetallics in Al–Si–Ti alloys. Journal of Alloys and Compounds, 2011, 509, 8013-8017.	5.5	43
69	Supportive strengthening role of Cr-rich phase on Al–Si multicomponent piston alloy at elevated temperature. Materials Science & Engineering A: Structural Materials: Properties, Microstructure and Processing, 2011, 528, 4427-4430.	5.6	59
70	Effect of existing form of alloying elements on the microhardness of Al–Si–Cu–Ni–Mg piston alloy. Materials Science & Engineering A: Structural Materials: Properties, Microstructure and Processing, 2011, 528, 5723-5728.	5.6	42
71	Quantitative comparison of three Ni-containing phases to the elevated-temperature properties of Al–Si piston alloys. Materials Science & Engineering A: Structural Materials: Properties, Microstructure and Processing, 2010, 527, 7132-7137.	5.6	168
72	Effects of trace C addition on the microstructure and refining efficiency of Al–Ti–B master alloy. Journal of Alloys and Compounds, 2010, 503, 286-290.	5.5	33

#	Article	IF	CITATIONS
73	Effect of co-addition of RE, Fe and Mn on the microstructure and performance of A390 alloy. Materials Science & Engineering A: Structural Materials: Properties, Microstructure and Processing, 2009, 527, 146-149.	5.6	27
74	Homogeneous Nucleation Catastrophe as a Kinetic Stability Limit for Superheated Crystal. Physical Review Letters, 1998, 80, 4474-4477.	7.8	229